

NASA TECHNICAL NOTE



NASA TN D-4897

C.1

NASA TN D-4897



LOAN COPY: RETURN TO
AFWL (WLIL-2)
KIRTLAND AFB, N MEX

TRANSIENT SOLIDIFICATION OUTSIDE A
COOLED PIPE WITH APPLICATION TO
A SOLAR BRAYTON HEAT RECEIVER

by Wellington W. Hu
Lewis Research Center
Cleveland, Ohio



NATIONAL AERONAUTICS AND SPACE ADMINISTRATION • WASHINGTON, D. C. • NOVEMBER 1968



0131590

NASA TN D-4897

TRANSIENT SOLIDIFICATION OUTSIDE A COOLED PIPE WITH
APPLICATION TO A SOLAR BRAYTON HEAT RECEIVER

By Wellington W. Hu

Lewis Research Center
Cleveland, Ohio

NATIONAL AERONAUTICS AND SPACE ADMINISTRATION

For sale by the Clearinghouse for Federal Scientific and Technical Information
Springfield, Virginia 22151 - CFSTI price \$3.00

ABSTRACT

The analysis involves time-variant heat conduction with the liquid-solid boundary moving radially through the axisymmetric heat-storage material as heat is transferred to the flowing cooling medium. Solutions were obtained by simultaneously solving the integrated nonlinear differential equations through numerical means. Quasi-steady radial heat conduction is utilized at an instant of time. Solutions for wall temperature, gas temperature, and solidification thickness along the tube for a 35-minute shadow portion of an Earth orbit are obtained for a solar Brayton heat receiver. A simplified solution neglecting the wall-temperature variation is also derived to compare with the numerical method.

TRANSIENT SOLIDIFICATION OUTSIDE A COOLED PIPE WITH APPLICATION TO A SOLAR BRAYTON HEAT RECEIVER

by Wellington W. Hu
Lewis Research Center

SUMMARY

A transient heat-transfer problem of solidification outside a cooled pipe is analyzed. This problem involves time-variant heat conduction with the liquid-solid boundary moving radially through the axisymmetric heat-storage material as heat is transferred to the flowing cooling medium. Heat-balance equations for the solidified material, the tube wall, and the cooling medium are derived. These nonlinear differential equations are solved simultaneously by using numerical integration. Quasi-steady radial heat conduction is utilized at each instant of time.

The analysis is applied to the solidification of heat-storage material in the heat receiver of a solar Brayton cycle space-power system. For this application, argon gas is the cooling medium and lithium fluoride is the heat-storage material. Solutions for wall temperature, gas temperature, and solidification thickness are presented for a 35-minute shadow portion of an Earth orbit. The effect of tube-entrance correction on heat transfer is also studied.

A simplified analysis that neglects the variation of wall temperature and heat-transfer coefficient along the tube is also developed. For a solar Brayton application, the simplified solution and the numerical method are compared graphically.

INTRODUCTION

Transient heat transfer for axisymmetric solidification outside a cooled pipe is analyzed. This time-variant heat-conduction problem considers a liquid-solid boundary moving radially as heat is transferred to the cooling medium flowing in the pipe. The analysis is applied to the solidification of heat-storage material in the heat receiver of a solar Brayton space-power system. The analysis is also applicable to other solar space-power systems, such as thermionic and thermoelectric, and to such problems as cylindri-

cal metal casting and ice formation outside a cooled pipe.

One-dimensional transient heat-conduction analyses with a change of phase have been developed (refs. 1 and 2) for a plane geometry. Axisymmetric heat conduction with a phase change considering freezing on a cylinder is analyzed in reference 3. The results of reference 3 are applied as local solutions at several stations along a tube. The computing time required to get a single station solution by the method of reference 3 is often large (sometimes 30 min). Therefore, a numerical analysis is developed in this report, which allows a direct solution for the whole tube in reduced computer time.

The analysis is demonstrated by obtaining solutions for a 30-tube solar Brayton heat receiver for a shadow period of 35 minutes. These solutions are plotted to show the variation of wall temperature, gas temperature, and frozen-material thickness and weight with position along the tube and time. In addition, the same calculations were performed by using heat-transfer coefficients that were corrected for tube entrance effects (ref. 4). A simplified solution neglecting the variation of wall temperature and heat-transfer coefficients along the tube is also developed for comparison with the numerical method.

SYMBOLS

c_p	specific heat, Btu/(lb mass)($^{\circ}$ R); J/(kg)(K)
D	diameter, ft; m
h	heat-transfer coefficient, Btu/(ft ²)(sec)($^{\circ}$ R); W/(m ²)(K)
h_F	heat of fusion, Btu/lb mass; J/kg
k	conductivity, Btu/(ft)(sec)($^{\circ}$ R); J/(m)(sec)(K)
L	length, ft; m
N	number of tubes
q	heat-transfer rate, Btu/sec; W
R	ratio of radius of frozen boundary to outside radius of inner tube
r	radius, ft; m
T	temperature, $^{\circ}$ R; K
V	velocity, ft/sec; m/sec
W	weight, lb mass; kg
w	total mass flow rate, lb mass/sec; kg/sec
X	scaled length, nondimensional

- x axial distance along tube length, ft; m
- μ absolute viscosity, (lb)(sec)/ft²; (N)(sec)/m²
- ρ density, lb mass/ft³; kg/m³
- τ time, sec
- ψ scaled time, nondimensional

Subscripts:

- av average
- B freezing boundary
- b bulk
- e entrance
- F fusion
- f film
- g fluid
- s solid
- w tube wall
- x axial distance
- 1 beginning of time interval
- 2 end of time interval

ANALYSIS

Numerical Integration Method

The thermal-energy-storage model considered herein is axisymmetric (fig. 1). The model considers a time-variant heat-conduction problem with the boundary between the molten liquid and the solid phase changing with time. The heat release from the latent heat of the storage material is conducted radially through the solid phase and convected to the heat-transfer fluid at the inner tube surface. Both ends of the tube are assumed to be insulated so that heat conduction is negligible. Furthermore, since the thermal conductivity of the tube wall is much higher than that of the storage material, which is a liquid, the temperature drop through the thin wall of the inner tube is assumed to be small enough to be neglected. The longitudinal conduction of heat is also neglected. The properties of the storage material are assumed to be invariant with slight temperature changes.

The quantity of frozen material is such that its freezing front will not reach the outer tube wall. A cooling fluid such as argon passed through the inner tube, with its temperature varying along the tube. Therefore, the heat-transfer coefficient based on the film temperature of the cooling fluid varies along the tube.

The equation for transient heat transfer in cylindrical coordinates is

$$\rho c_p \frac{\partial T}{\partial \tau} = \frac{k}{r} \frac{\partial}{\partial r} \left(r \frac{\partial T}{\partial r} \right) \quad (1)$$

For any differential time interval $d\tau$, the heat balance in any differential section dx along the cylindrical wall can be treated as quasi-steady radial heat conduction. The latent heat due to the change of phase from liquid to solid plus the sensible heat due to the temperature drop of the solid equals the heat transfer from the wall to the cooling fluid. The equation for this heat balance, derived in the appendix, is as follows

$$\rho_s h_F (2\pi r_B) dx \frac{dr_B}{d\tau} + \left[(c_p)_s T_B \rho_s (2\pi r_B) dx \frac{dr_B}{d\tau} - \rho_s (c_p)_s 2\pi dx \frac{\partial}{\partial \tau} \int_{r_w}^{r_B} r T_s dr \right] = 2\pi k_s dx \frac{T_B - T_w}{\ln \frac{r_B}{r_w}} \quad (A8)$$

where r_w is the radius of the inner tube, neglecting tube wall thickness, r_B is the radius at the frozen boundary, and T_B is the melting temperature of the solid. Here T_w , T_s , and r_B are functions of time τ and the axial distance x . Because the temperature difference for subcooling of the solid is small, the change of the sensible heat of the solid phase is much smaller than that of the latent heat. For a first approximation, the temperature distribution inside the solid is assumed to be linear. For the more precise case, the logarithmic temperature distribution is used in the derivation (see appendix). The final integrated equation with the linear temperature distribution in the solid is as follows

$$\begin{aligned}
& \frac{2\Delta\tau}{r_w^2} (2T_B - T_{w,1} - T_{w,2}) - \frac{2}{3} \frac{\rho_s (c_p)}{k_s} (\ln R_{B,av}) \left[T_B (R_{B,2} - R_{B,1}) (R_{B,2} + R_{B,1} + 1) \right. \\
& \quad \left. - T_{w,2} (R_{B,2} - 1) (R_{B,2} + 2) + T_{w,1} (R_{B,1} - 1) (R_{B,1} + 2) \right] \\
& \quad = \frac{\rho_s h_F}{k_s} \left[R_{B,2}^2 (\ln R_{B,2}^2 - 1) - R_{B,1}^2 (\ln R_{B,1}^2 - 1) \right] \quad (A15)
\end{aligned}$$

where

$$\Delta\tau = \tau_2 - \tau_1$$

The heat balance between the thermal-storage material and the gas at any time τ and any portion x is given in the following equation

$$q = 2\pi k_s dx \frac{T_B - T_w}{\ln R_B} = h_g (2\pi r_w) dx (T_w - T_g) \quad (2a)$$

where

$$\frac{T_B - T_w}{\ln R_B} = \frac{r_w h_g}{k_s} (T_w - T_g) \quad (2b)$$

Writing equation (2b) explicitly for T_w gives

$$T_w = \frac{T_B + \frac{r_w h_g \ln R_B}{k_s} T_g}{\frac{r_w h_g \ln R_B}{k_s} + 1} \quad (2c)$$

The heat-transfer rate through the wall at any time τ to the gas is equal to the rate of increase of enthalpy in the gas

$$\frac{w(c_p)_g}{N} \frac{\partial T_g}{\partial x} = \pi D_w h_g (T_w - T_g) \quad (3a)$$

where both the heat-transfer coefficient h_g and the temperature of gas or sink, are functions of time τ and length x . Integrating equation (3a) with respect to x and using the average value of $h_g(T_w - T_g)$ over increments of Δx in the difference equation at any time τ give:

$$T_{g, x+\Delta x} - T_{g, x} = \frac{ND_w}{w(c_p)_g} \frac{\Delta x}{2} \left[h_{g, x}(T_{w, x} - T_{g, x}) + h_{g, x+\Delta x}(T_{w, x+\Delta x} - T_{g, x+\Delta x}) \right] \quad (3b)$$

A rearrangement of equation (3b) gives the following equation for the gas temperature at the station $x + \Delta x$:

$$T_{g, x+\Delta x} = \frac{T_{g, x} + \frac{N\pi D_w \Delta x}{2w(c_p)_g} \left[h_{g, x}(T_{w, x} - T_{g, x}) + h_{g, x+\Delta x} T_{w, x+\Delta x} \right]}{1 + \frac{N\pi D_w \Delta x h_{g, x+\Delta x}}{2w(c_p)_g}} \quad (4)$$

In equation (4), the heat-transfer coefficient is a function of temperature and, therefore, a function of axial position x and time τ .

At the beginning of the tube, that is, at $x = 0$, and any time τ , the inlet fluid temperature $T_g(0, \tau) = T_{g, e}$ is constant and known. The wall temperature T_w , the frozen radius ratio $R_{B, 2}$ and heat-transfer coefficient $h_g(0, \tau)$ can be calculated by using equations (A15), (2), and the heat-transfer equation valid to the specific application.

The calculation is started at $x = 0$, with a known value of $h_g(0, 0)$ to obtain $h_g(0, \tau)$ by iteration procedures. Then at constant time τ the calculation along the tube axis is started at $x = 0$. Values of $T_{w, x+\Delta x}$ and $T_{g, x+\Delta x}$ are estimated by using the h_g obtained at the beginning of the increment. Based on these estimated wall and fluid temperatures, equations (A15), (2), (4), and the applicable heat-transfer equation are used to obtain the values of $T_{w, x+\Delta x}$, $T_{g, x+\Delta x}$, $h_{g, x+\Delta x, \tau}$, and $R_{B, x+\Delta x}$. Final values of these parameters are obtained by iteration procedures until h_g is obtained within a specific limit.

The simultaneous equations (A15), (2), and (4) are solved by using a stepwise approximation method and are programmed in FORTRAN IV for the IBM-7094 computer.

Simplified Solution

As mentioned in the previous section, the sensible heat of the solid is a small quantity for the range of R_B considered and, therefore, was neglected. This leads to the development of a simplified solution. The tube wall temperature is assumed to be constant and equal to the melting point of the heat-storage material (i. e., infinite conductivity of the frozen material is assumed). Then the fluid temperature is not a function of time. The heat-balance equation between the frozen front and the cold sink is

$$2\pi r_B \rho_S dx h_F \frac{\partial r_B}{\partial \tau} = 2\pi r_w dx h_g (T_w - T_g) \quad (5)$$

Let $R_B = r_B/r_w$ and simplify equation (5):

$$R_B \frac{dR_B}{d\tau} = \frac{h_g}{r_w \rho_S h_F} (T_w - T_g) \quad (6)$$

Integrating equation (6) from $\tau = 0$ to τ gives

$$R_{B,2}^2 - 1 = \frac{2h_g}{r_w \rho_S h_F} (T_w - T_g) \tau \quad (7)$$

where T_w is constant and equal to T_B . The heat-transfer rate through the wall to the gas is equal to the rate of increase of enthalpy of the gas, as follows:

$$\frac{w}{N} (c_p)_g \frac{dT_g}{dx} = 2\pi r_w h_g (T_w - T_{g,x}) \quad (8)$$

Assuming the heat-transfer coefficient to be constant and equal to an average value and integrating equation (8) with respect to x , yield

$$\left(\frac{T_w - T_{g,e}}{T_w - T_{g,x}} \right) = \exp \left[\frac{2\pi r_w N h_g x}{w (c_p)_g} \right] \quad (9a)$$

or

$$T_{g,x} = T_w - \frac{T_w - T_{g,e}}{\exp\left[\frac{2\pi r_w N h_g x}{w(c_p)_g}\right]} \quad (9b)$$

Substituting equation (9a) into equation (7) gives

$$R_B^2(x, \tau) - 1 = \frac{2h_g \tau}{r_w \rho_s h_F} (T_w - T_{g,e}) \exp\left[\frac{2\pi r_w h_g x}{w(c_p)_s}\right] \quad (10a)$$

$$R_B^2(x, \tau) - 1 = \psi e^{-X} \quad (10b)$$

where

$$X = \frac{2\pi r_w N h_g x}{w(c_p)_g}$$

$$\psi = \frac{2h_g (T_B - T_{g,e}) \tau}{r_w \rho_s h_F}$$

Application

The particular application investigated herein is the solidification of the heat-storage material in the heat receiver of a solar Brayton space-power system (fig. 2). During the sunlight period of an eclipsed orbit, solar heat melts the storage material. A paraboloidal mirror supplies solar thermal energy by focusing the Sun's rays through an aperture onto the cavity wall where the heat-storage material is stored inside concentric tubes (fig. 3). Argon gas passes through the inner tube and extracts heat for use by the power conversion system. During the shadow period of 35 minutes, the gas absorbs the latent heat of fusion as the storage material freezes. The transient heat conduction through the axisymmetric body of the heat-storage material along the tube is solved by the analysis just presented. The reference conditions used in the calculations for a 30-tube heat receiver for a solar Brayton system are shown in table I. Lithium fluoride is used as the heat-storage material. References 4 and 5 present data for gas heat-transfer coefficients

under moderately high heat flux conditions. For the application considered herein, the Reynolds number falls in the region of transition flow. The test data for the heat-transfer coefficient of reference 4 are scattered, but an average curve for these data can be represented by the following equation:

$$h_g = 0.00080 \frac{k_f}{D_w} \left(\frac{\rho_f V_b D_w}{\mu_f} \right)^{1.15} \left[\frac{(c_p)_f \mu_f}{k_f} \right]^{0.4} \quad (11)$$

All properties of the fluid are based on the film temperature which is

$$T_f = \frac{1}{2} (T_w + T_g)$$

The entrance correction factor for the heat-transfer coefficient in the transition flow is less prominent than that in the turbulent flow. For the worst condition, the entrance correction factor in the turbulent flow region is obtained from the data of figure 10 of reference 4 and applied to an entrance length of the tube equal to 10 times the tube inner diameter.

Since the sensible heat of the solid-storage material is small, the use of a linear temperature distribution instead of a logarithmic temperature distribution results in a negligible error. Therefore, equation (A15) was used for the calculations.

Equations (A15), (2), (4), and (11) are used to solve for h_g , R_B , T_w , and T_g . These equations need to be solved simultaneously and therefore a computer is used to obtain the solution. For this purpose, the tube was divided into 50 increments. An increase in the number of increments from 50 to 100 along the tube axis did not change the solution in the fourth decimal, and neither did a time interval of less than 40 seconds.

RESULTS AND DISCUSSION FOR A SOLAR BRAYTON APPLICATION

Results of Numerical Integration Method With and Without Tube Entrance Correction

Figure 4 shows the variation of ratio of frozen radius to inner tube radius along the length of tube at two different times. The tube diameter is 0.087 foot (0.026 m), and the length is 12.5 feet (3.81 m) which is divided into 50 equal increments bounded by station numbers from 1 to 51. The frozen depth can be calculated by the following equation:

$$L_F = (R_B - 1)r_1$$

At the end of a shadow period of about 35 minutes, the frozen depth at the entrance with the tube entrance correction is about eight times that at the exit (hot end). This suggests that more thermal storage material is required at the entrance.

The ratio of frozen radius to the inner tube radius is about 1.5 without correction, while it is 2.02 with the entrance correction for the first station at the end of 35.5 minutes of shadow period of the orbit. This increase of frozen radius ratio will require more thermal-storage material at the entrance of the tube. However, the entrance effects, as shown in figure 4, diminish rapidly after the third station. In order to avoid oversizing the receiver, the outside tube near the tube entrance could be made to follow the contour of the frozen-radius curve without entrance correction (fig. 4); then after about 15 minutes of the shadow period, the frozen radius at the entrance section would reach the outside tube. The result is to decrease the outlet gas temperature about 2° R (1.1 K). Such a small temperature variation can be tolerated by the Brayton power system.

Figure 5 shows the variation of the wall temperature along the length of the tube at three different times. Without the tube entrance correction, the calculated wall temperature drop at station 1 (at the cold end) is about 12° R (6.5 K) from the beginning at time zero to the end of the 35-minute shadow period. However, when the entrance correction is considered, the wall temperature at station 1 at the end of 35 minutes of shadow period drops about 50° R (27.8 K) from the postulated starting value at time zero.

The effect of the entrance correction is also displayed in figure 6, which shows the temporal variation in wall temperature at the tube entrance and exit. Although the entrance correction increases wall-temperature drop at the tube entrance from 12° to 50° R (6.5 to 27.8 K), this effect is markedly attenuated at the tube exit, and exit wall temperature varies less than 0.5° R (0.28 K) as a result of the entrance correction. Figure 7 shows the weight distribution of thermal-storage material along the length of the tube for several shadow times. At station 1, the entrance effect increases the freezing weight per unit tube length to 2.5 times that without correction. Figure 8 shows that the variation of total frozen weight of lithium fluoride as a function of time is less with the entrance correction than without the correction. Since the freezing solid grows much faster in the entrance region with the correction, the solid phase transfers relatively more sensible heat and less heat of fusion than is the case without correction for the entrance effects. At the same time, the gas temperature becomes higher in the later stations of the tube with the entrance correction so that it absorbs less heat of fusion and thus reduces the total freezing weight. Because the temperature of gas at the exit is higher with the entrance correction, more heat is transferred. This additional amount of heat is from the sensible heat of cooling rather than from the heat of fusion.

Simplified Solution

The results of the simplified solution are shown in figures 9 to 11 plotted with those of the numerical integration method for comparison. Figure 9 shows that the frozen radius ratio R_B obtained from the simplified solution is lower at the front stations and higher at later stations along the tube. In this figure, the temperature of the wall is assumed to be constant and the heat-transfer coefficient is assumed to be an average of the heat-transfer coefficients obtained at time zero along the tube axis. This average value of heat-transfer coefficient is 0.001581 Btu per square foot per second per $^{\circ}\text{R}$ ($32.3 \text{ W}/(\text{m}^2)(\text{K})$).

Figure 10 shows that the effect of entrance correction was to increase the frozen radius ratio nearly 30 percent at station 1 at the end of 35 minutes of shadow period. At a later station, such as 26, the gas had a higher temperature due to the entrance effect. The wall temperature was also higher. Therefore, the value of frozen radius ratio is reduced by the entrance correction. The maximum difference of the frozen radius ratio at the tube entrance is 3 percent less in the simplified solution (also shown in fig. 10).

Figure 11 shows variation of gas temperature along the length of the tube. At the end of 35 minutes of shadow period, the gas temperature at the exit decreased from time zero only about 1°R (0.56 K) with no entrance correction considered for the 30-tube solar heat receiver. This relatively small variation in outlet gas temperature is acceptable because the power output of the system would vary less than 1 percent as a consequence of the temperature change. With the tube entrance correction, the outlet gas temperature increased about 2.8°R (1.5 K) at time $\tau = 0$.

The gas temperature obtained from the simplified solution is always lower than that obtained by using the numerical integration method (see fig. 11). The maximum difference of gas temperatures is only about 10°R (5.5 K) and occurs approximately at station 20. The local heat-transfer coefficient used in the numerical integration method is greater than the average value used with the simplified solution from the tube entrance to station 20. Thereafter, the average value of heat-transfer coefficient exceeds the local value obtained by the numerical integration method. This results from the decrease in Reynolds number at the tube exit where the gas is hot, because of the change in gas properties.

Suggestions for Design of Heat Receiver

The curve for frozen radius ratio R_B from the transient heat analysis suggests the use of a tapered outside tube to store more thermal storage material in the entrance portion of the tube. For the proper distribution of lithium fluoride weight at all the stations along the tube, the outside tube can be made with a taper ratio of about 1.4, with rings to

separate lithium fluoride into different compartments, as shown in figure 12.

The outlet gas temperature at the end of a shadow period of 35 minutes is only 1.4°R (0.7 K) below the initial tube exit value (fig. 11). For the same mass flow and tube length, an increase in diameter of 12 percent results in a decrease of the exit gas temperature of about 3.6°R (2 K) for the 30-tube receiver. For the same length and diameter, but an increased number of tubes from 30 to 50, the heat-transfer area per unit mass flow will increase and, therefore, the exit gas temperature will increase (from 1951.8° to 1965.8°R (1084.3 to 1092.1 K)) about 14°R (7.8 K) or 0.7 percent for the same flow situation. Similarly, a 3.6-percent reduction in tube length from 12.5 to 12.05 feet (3.81 to 3.66 m) will decrease exit gas temperature by 5.4°R (3.0 K); thus, a given fractional change in tube length has a greater effect on exit gas temperature than does a change in number of tubes.

CONCLUSION

This analysis investigated the solidification outside a cooled pipe with application to the receiver design for a solar Brayton cycle space-power system. The thermal-storage material surrounding the heat receiver tubes has an axisymmetric shape. The heat-transfer problem in the receiver is a time-variant heat-conduction problem with the liquid-solid boundary moving through the thermal-storage material during the shadow portion of an orbit. The solution also applies in general to a problem such as metal casting and ice formation, with variable wall temperature and heat flux along the tube.

From the heat-receiver analysis, the ratio of frozen radius to the inner tube radius, the wall temperature, and the gas exit temperature are solved by the Lewis IBM 7094 computer in less than 2 minutes of computing time. At the end of the 35-minute shadow period, the gas exit temperature decreased only 1.4°R (0.7 K) below the exit temperature value at time zero.

The frozen radius ratio along the tube axis is less than 2, and the weight distribution curve suggests a tapered design for the thermal-storage device.

A fractional increase in tube length is more effective in increasing the gas exit temperature than is an increase in the number of tubes.

Lewis Research Center,
National Aeronautics and Space Administration,
Cleveland, Ohio, August 2, 1968,
120-33-07-03-22.

APPENDIX - DERIVATION OF EQUATIONS OF HEAT BALANCE BETWEEN SOLID PHASE AND COOLING WALL

The governing equation of the transient heat transfer in cylindrical coordinates is

$$\rho_s c_p \frac{\partial T}{\partial \tau} = \frac{k_s}{r} \frac{\partial}{\partial r} \left(r \frac{\partial T}{\partial r} \right) \quad (\text{A1a})$$

or

$$\rho_s (c_p)_s r \frac{\partial T}{\partial \tau} = k_s \frac{\partial}{\partial r} \left(r \frac{\partial T}{\partial r} \right) \quad (\text{A1b})$$

Integration from the inner radius to the freezing boundary results in

$$\rho_s (c_p)_s \int_{r_w}^{r_B} r \frac{\partial T}{\partial \tau} dr = k_s \left(r_B \frac{\partial T}{\partial r} \Big|_{r_B} - r_w \frac{\partial T}{\partial r} \Big|_{r_w} \right) \quad (\text{A2})$$

The heat balance at the freezing boundary is

$$\rho_s h_F \frac{dr_B}{d\tau} = k_s \frac{\partial T}{\partial r} \Big|_{r_B} \quad (\text{A3})$$

Since

$$\frac{\partial}{\partial \tau} \int_{r_w}^{r_B} r T dr = \int_{r_w}^{r_B} r \frac{\partial T}{\partial \tau} dr + r_B T_B \frac{dr_B}{d\tau} \quad (\text{A4})$$

substitute equations (A3) and (A4) into equation (A2) to obtain

$$\rho_s r_B h_F \frac{dr_B}{d\tau} + \rho_s (c_p)_s r_B T_B \frac{dr_B}{d\tau} - \rho_s (c_p)_s \frac{\partial}{\partial \tau} \int_{r_w}^{r_B} r T dr = k_s r_w \frac{\partial T}{\partial r} \Big|_{r_w} \quad (\text{A5})$$

Multiply both sides of equation (A5) by $2\pi dx$

$$\rho_B h_F 2\pi dx \frac{dr_B}{d\tau} + \rho_S (c_p)_S 2\pi r_B dx T_B \frac{dr_B}{d\tau} - \rho_S (c_p)_S 2\pi dx \frac{\partial}{\partial \tau} \int_{r_w}^{r_B} r T dr = k_S 2\pi r_w dx \left. \frac{\partial T}{\partial r} \right|_{r_w} \quad (A6)$$

For a differential time interval, the heat transfer across the cylindrical wall can be treated as quasi-steady radial heat conduction. Then

$$r_w \left. \frac{\partial T}{\partial r} \right|_{r_w} = \frac{T_B - T_w}{\ln \left(\frac{r_B}{r_w} \right)} \quad (A7)$$

Substituting equation (A7) into equation (A6) gives equation (A2):

$$\rho_S h_F (2\pi r_B) dx \frac{dr_B}{d\tau} + \left[(c_p)_S T_B \rho_S (2\pi r_B) dx \frac{dr_B}{d\tau} - \rho_S (c_p)_S 2\pi dx \frac{\partial}{\partial \tau} \int_{r_w}^{r_B} r T_S dr \right] = 2\pi k_S dx \frac{T_B - T_w}{\ln \left(\frac{r_B}{r_w} \right)} \quad (A8)$$

Eliminate $2\pi dx$ from both sides of equation (A8). Let $R = r/r_w$, and multiply by $d\tau$

$$\rho_S h_F R_B dR_B + (c_p)_S T_B \rho_S R_B dR_B - \rho_S (c_p)_S \partial \int_1^{R_B} R T_S dR = \frac{k_S}{r_w^2} \frac{T_B - T_w}{\ln R_B} d\tau$$

Then multiply by $\ln R_B$

$$\rho_s h_F R_B \ln R_B dR_B + \rho_s (c_p)_s T_B \ln R_B R_B dR_B - \rho_s (c_p)_s \ln R_B d \int_1^{R_B} RT_s dR$$

$$= \frac{k_s (T_B - T_w)}{r_w^2} d\tau$$

Integrating and rearranging terms give

$$\int_{\tau_1}^{\tau_2} \frac{T_B - T_w}{r_w^2} d\tau - \frac{\rho_s (c_p)_s}{k_s} \left(T_B \int_{R_{B,1}}^{R_{B,2}} R_B \ln R_B dR_B \right. \\ \left. - \int_{R_{B,1}}^{R_{B,2}} \ln R_B d \int_1^{R_B} RT_s dR \right) = \frac{\rho_s h_F}{k_s} \int_{R_{B,1}}^{R_{B,2}} R_B \ln R_B dR_B \quad (A9)$$

Integrate by parts to the following term

$$\int_{R_{B,1}}^{R_{B,2}} \ln R_B d \int_1^{R_B} RT_s dR$$

$$= \ln R_{B,2} \int_1^{R_{B,2}} RT_s dR - \ln R_{B,1} \int_1^{R_{B,1}} RT_s dR - \int_{R_{B,1}}^{R_{B,2}} \frac{1}{R_B} \int_1^{R_B} RT_s dR dR_B$$

(A10a)

Substitute in equation (A9)

$$\begin{aligned}
& \int_{\tau_1}^{\tau_2} \frac{T_B - T_w}{r_w^2} d\tau - \frac{\rho_s (c_p)_s}{k_s} \left(T_B \int_{R_{B,1}}^{R_{B,2}} R_B \ln R_B dR_B \right. \\
& + \int_{R_{B,1}}^{R_{B,2}} \frac{1}{R_B} \int_1^{R_B} R T_s dR dR_B - \ln R_{B,2} \int_1^{R_{B,2}} R T_s dR \\
& \left. + \ln R_{B,1} \int_1^{R_{B,1}} R T_s dR \right) = \frac{\rho_s h_F}{k_s} \int_{R_{B,1}}^{R_{B,2}} R_B \ln R_B dR_B \quad (A10b)
\end{aligned}$$

For the quasi-steady radial heat conduction, the temperature distribution inside the solid cylindrical frozen material is

$$T_s = c \ln R + T_w$$

where

$$c = \frac{T_B - T_w}{\ln R_B}$$

Then

$$\begin{aligned}
\int_1^{R_B} R T_s dR &= \int_1^{R_B} R (c \ln R + T_w) dR = \left(\frac{c}{2} R_B^2 \ln R_B - c \frac{R_B^2 - 1}{4} + T_w \frac{R_B^2 - 1}{2} \right) \\
&= T_B \left(\frac{R_B^2}{2} - \frac{R_B^2 - 1}{4 \ln R_B} \right) + T_w \left(\frac{R_B^2 - 1}{4 \ln R_B} - \frac{1}{2} \right) \quad (A11)
\end{aligned}$$

By the relation of equation (A11), evaluate the first two terms on the right side of equation (A10a)

$$\begin{aligned}
& \ln R_{B,2} \int_1^{R_{B,2}} R T_s dR - \ln R_{B,1} \int_1^{R_{B,1}} R T_s dR \\
&= T_B \left(\frac{R_{B,2}^2}{2} \ln R_{B,2} - \frac{R_{B,2}^2}{4} - \frac{R_{B,1}^2}{2} \ln R_{B,1} + \frac{R_{B,1}^2}{4} \right) \\
&+ T_{w,2} \left(\frac{R_{B,2}^2 - 1}{4} - \frac{\ln R_{B,2}}{2} \right) - T_{w,1} \left(\frac{R_{B,1}^2 - 1}{4} - \frac{\ln R_{B,1}}{2} \right) \quad (A12a)
\end{aligned}$$

and also,

$$\begin{aligned}
& \int_{R_{B,1}}^{R_{B,2}} \frac{1}{R_B} \int_1^{R_B} R T_s dR dR_B \\
&= \int_{R_{B,1}}^{R_{B,2}} \left[T_B \left(\frac{R_B}{2} - \frac{R_B^2 - 1}{4R_B \ln R_B} \right) + T_w \left(\frac{R_B^2 - 1}{4R_B \ln R_B} - \frac{1}{2R_B} \right) \right] dR_B \\
&= \frac{T_B}{4} \left\{ R_{B,2}^2 - R_{B,1}^2 + \left[\ln(\ln R_{B,2}) - \ln(\ln R_{B,1}) \right] - \frac{R_{B,2}^2 - R_{B,1}^2}{2(\ln R_B)_{av}} \right\} \\
&+ \frac{T_{w,2} + T_{w,1}}{4} \left\{ -\frac{1}{2} \left[\ln(\ln R_{B,2}) - \ln(\ln R_{B,1}) \right] + \frac{R_{B,2}^2 - R_{B,1}^2}{4 \ln(R_B)_{av}} - (\ln R_{B,2} - \ln R_{B,1}) \right\} \quad (A12b)
\end{aligned}$$

where

$$\ln(R_B)_{av} = \frac{1}{2} (\ln R_{B,2} + \ln R_{B,1})$$

is introduced in the integration to avoid the use of a power series.

Substitute equations (A12a) and (A12b) into the equation (A9a) and multiply by 4. Then equation (A10b) becomes

$$\begin{aligned} & \frac{2\Delta T}{r_w^2} (2T_B - T_{w,1} - T_{w,2}) - \frac{\rho_s (c_p)_s}{k_s} \left(T_B \left\{ R_{B,2}^2 - R_{B,1}^2 \right. \right. \\ & \left. \left. + \left[\ln(\ln R_{B,2}) - \ln(\ln R_{B,1}) \right] - \frac{R_{B,2}^2 - R_{B,1}^2}{2 \ln(R_B)_{av}} \right\} \right. \\ & \left. - T_{w,2} \left\{ R_{B,2}^2 - 1 + \frac{1}{2} \left[\ln(\ln R_{B,2}) - \ln(\ln R_{B,1}) \right] - \frac{R_{B,2}^2 - R_{B,1}^2}{4 \ln(R_B)_{av}} - (\ln R_{B,2} + \ln R_{B,1}) \right\} \right. \\ & \left. + T_{w,1} \left\{ R_{B,1}^2 - 1 - \frac{1}{2} \left[\ln(\ln R_{B,2}) - \ln(\ln R_{B,1}) \right] + \frac{R_{B,2}^2 - R_{B,1}^2}{4 \ln(R_B)_{av}} - (\ln R_{B,2} + \ln R_{B,1}) \right\} \right) \\ & = \frac{\rho_s h_F}{k_s} \left[R_{B,2}^2 (\ln R_{B,2}^2 - 1) - R_{B,1}^2 (\ln R_{B,1}^2 - 1) \right] \end{aligned} \quad (A13)$$

The sensible heat-drop term of the solid in equation (A12b) is very lengthy. This term is small compared with the heat-of-fusion term, so that the linear temperature distribution inside the solid phase can be assumed with negligible error. The linear relation is

$$T_s = T_w + \frac{T_B - T_w}{R_B - 1} (R - 1) \quad (A14)$$

Then equation (A9) becomes

$$\begin{aligned}
& \frac{2\Delta T}{r_w^2} (2T_B - T_{w,1} - T_{w,2}) - \frac{2}{3} \frac{\rho_s (c_p)_s}{k_s} (\ln R_{B,av}) \left[T_B (R_{B,2} - R_{B,1})(R_{B,2} + R_{B,1} + 1) \right. \\
& \quad \left. - T_{w,2} (R_{B,2} - 1)(R_{B,2} + 2) + T_{w,1} (R_{B,1} - 1)(R_{B,1} + 2) \right] \\
& \quad = \frac{\rho_s h_F}{k_s} \left[R_{B,2}^2 (\ln R_{B,2}^2 - 1) - R_{B,1}^2 (\ln R_{B,1}^2 - 1) \right] \tag{A15}
\end{aligned}$$

REFERENCES

1. Cullom, Richard R. ; Robbins, William H. ; and Todd, Carroll A. : One-dimensional Heat-Transfer Analysis of Thermal-Energy Storage for Solar Direct-Energy-Conversion Systems. NASA TN D-2119, 1964.
2. Siegel, Robert; and Savino, Joseph M. : An Analysis of the Transient Solidification of a Flowing Warm Liquid on a Convective Cooled Wall. Proceedings of the Third International Heat Transfer Conference. Vol. 4. AIChE, 1966, pp. 141-151.
3. Cullom, Richard R. ; Diedrich, George; and Albers, Lynn U. : Analysis of Solidification in Thermal-Energy Storage Systems with Axisymmetric Heat-Transfer Solutions. NASA TN D-3763, 1966.
4. Deissler, R. G. : Turbulent Heat Transfer and Friction in the Entrance Regions of Smooth Passages. Trans. ASME, vol. 77, no. 8, Nov. 1955, pp. 1221-1233.
5. Humble, Leroy V. ; Lowdermilk, Warren H. ; and Desmon, Leland G. : Measurements of Average Heat-Transfer and Friction Coefficients for Subsonic Flow of Air in Smooth Tubes at High Surface and Fluid Temperatures. NACA Rept. 1020, 1951.
6. Weiland, Walter F. ; and Lowdermilk, Warren H. : Measurements of Heat-Transfer and Friction Coefficients for Air Flowing in a Tube of Length-Diameter Ratio of 15 at High Surface Temperatures. NACA RM E53E04, 1953.
7. Svehla, Roger A. : Estimated Viscosities and Thermal Conductivities of Gases at High Temperature. NASA TR R-132, 1962.
8. Anon. : A Compendium of Data on Lithium and Selected Compounds of Lithium. Lithium Corp. of America, Inc., July 1959.

TABLE I. - REFERENCE CONDITIONS AND PROPERTIES USED
IN COMPUTER CALCULATIONS

Argon^a:	
Mass flow rate, lb mass/sec; kg/sec	0.621; 0.28
Gas temperature at inlet to receiver, °R; K	1457; 809
Gas temperature at outlet from receiver, °R; K	1950; 1083
Inlet pressure of gas, lb force/ft ² ; N/m ²	1965.6; 94 000
Pressure drop, percent of inlet pressure	2
Shadow portion of 96-min orbit time, min	35
Lithium fluoride^b:	
Molecular weight	25.94
Melting point, °R; K	2020; 1122
Density of solid at 505° R (280 K), lb mass/ft ³ ; kg/m ³	165; 2640
Conductivity of solid at 2020° R (1122 K), Btu/(hr)(ft)(°R); W/(m)(K)	5; 8.65
Specific heat of solid at 2020° R (1122 K), Btu/(lb mass)(°R); kJ/(kg)(K)	0.581; 2.43
Heat of fusion, Btu/lb; kJ/kg	450; 1047

^aProperties from ref. 7.

^bData from ref. 8.

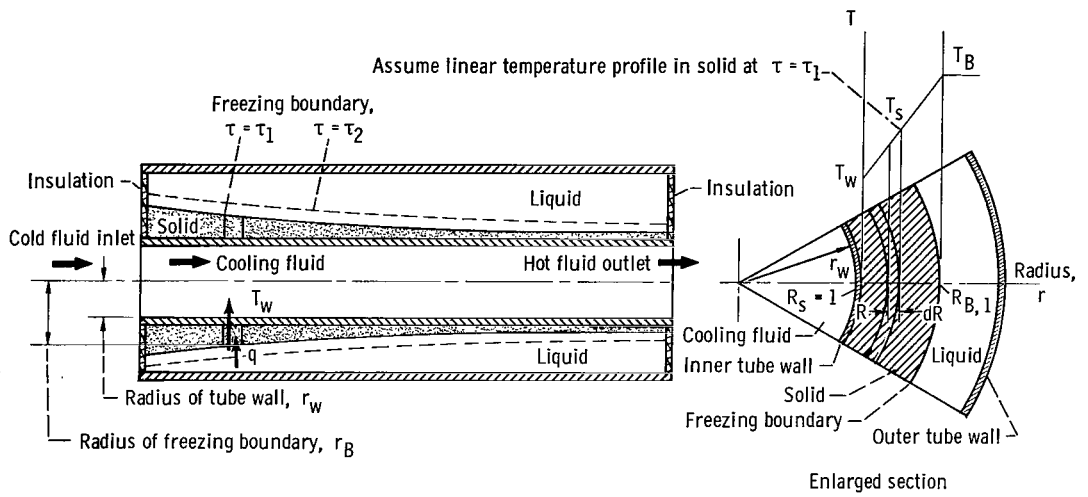
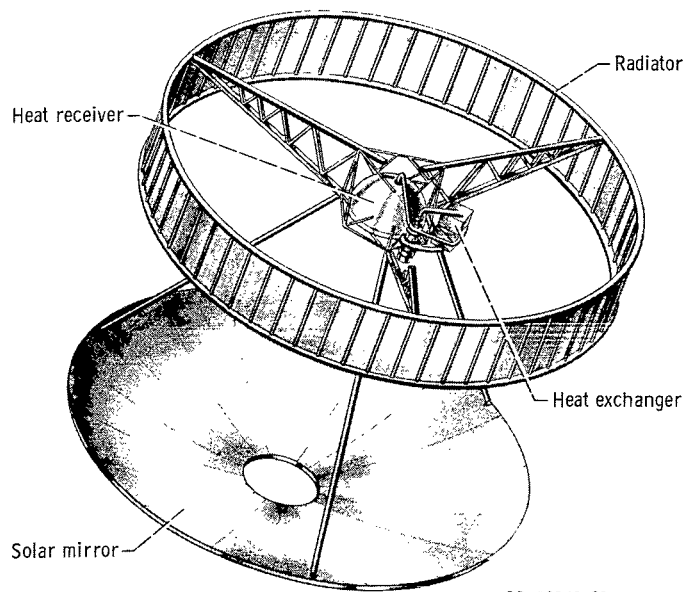


Figure 1. - Thermal-energy-storage model.

CD-9990-33



CD-10069-31

Figure 2. - Sketch of solar Brayton space powerplant.

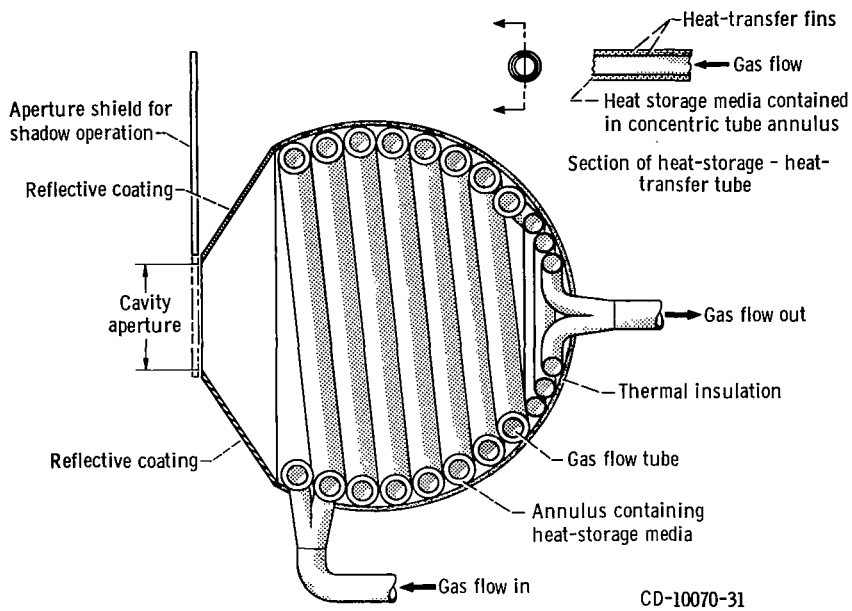


Figure 3. - Sketch of solar heat receiver.

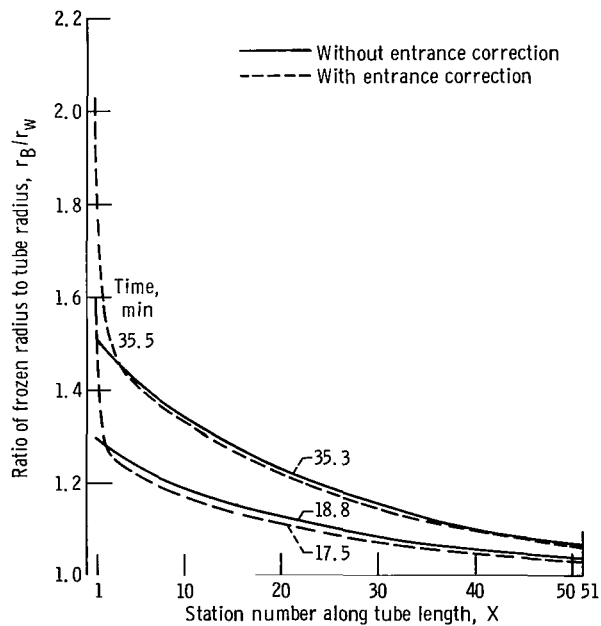


Figure 4. - Ratio of frozen radius to tube radius at different stations along tube with and without entrance correction. Tube length, 12.5 feet (3.81 m); tube diameter, 0.087 foot (0.026 m); number of tubes, 30.

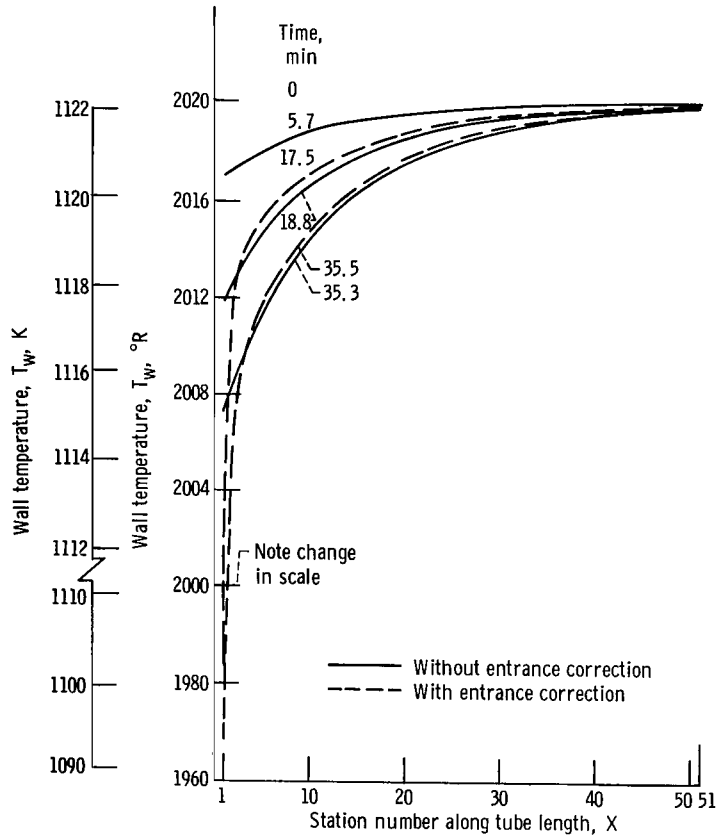


Figure 5. - Wall temperature at different stations along tube axis with and without entrance correction. Tube length, 12.5 feet (3.81 m); tube diameter, 0.087 foot (0.026 m); number of tubes, 30.

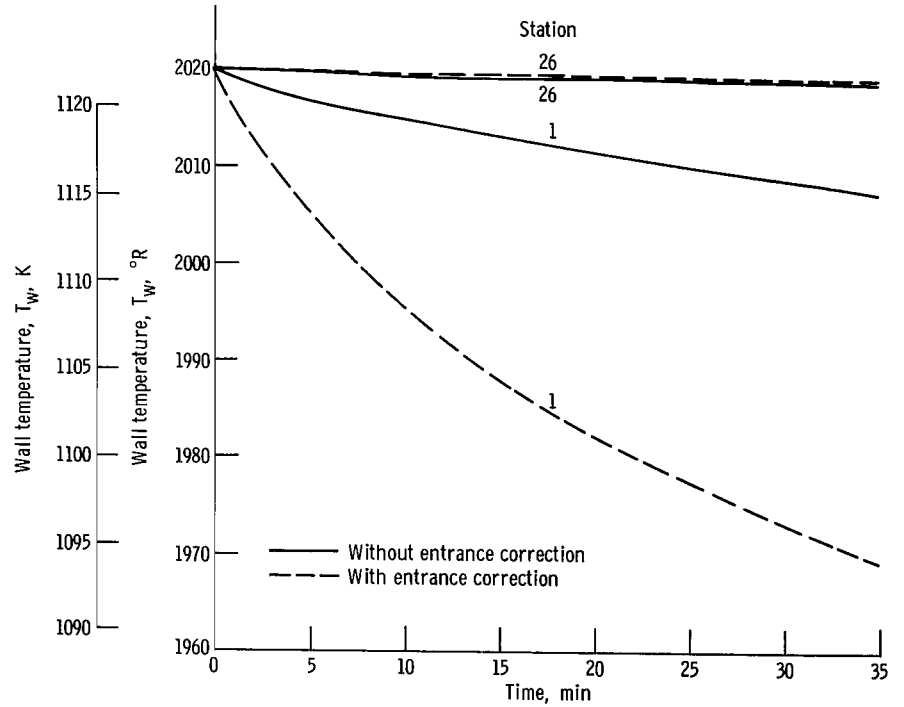


Figure 6. - Variation of wall temperature with time with and without entrance correction. Tube length, 12.502 feet (3.81 m); tube diameter, 0.087 foot (0.026 m); number of tubes, 30.

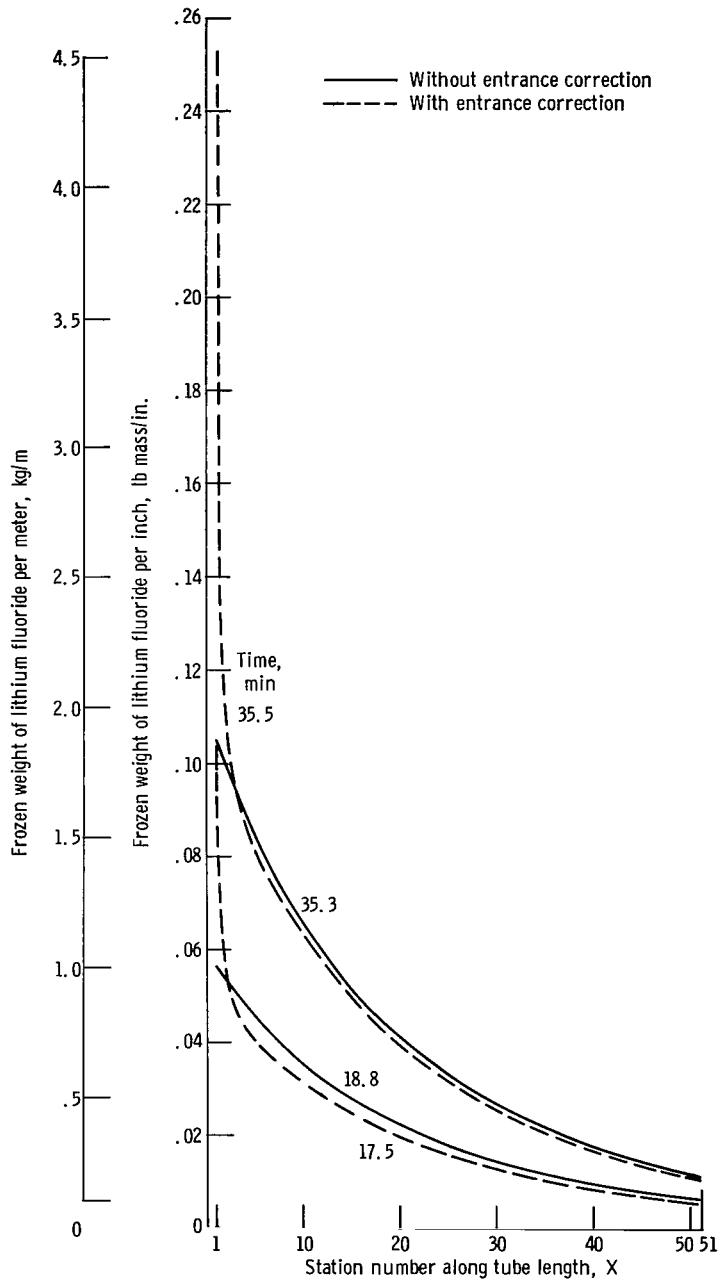
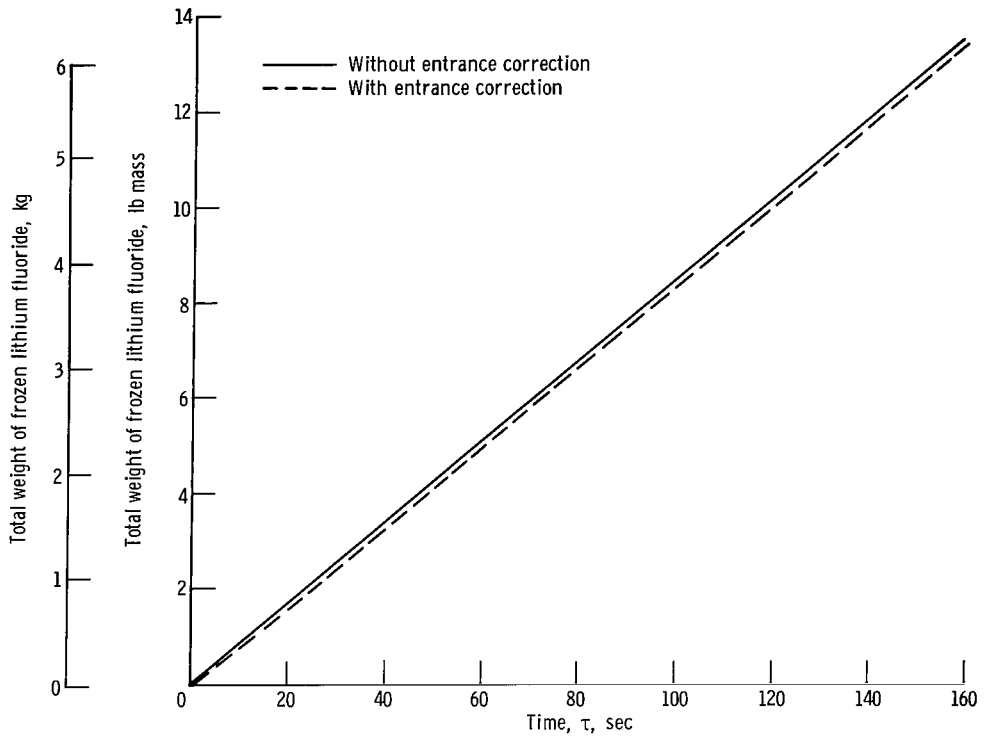
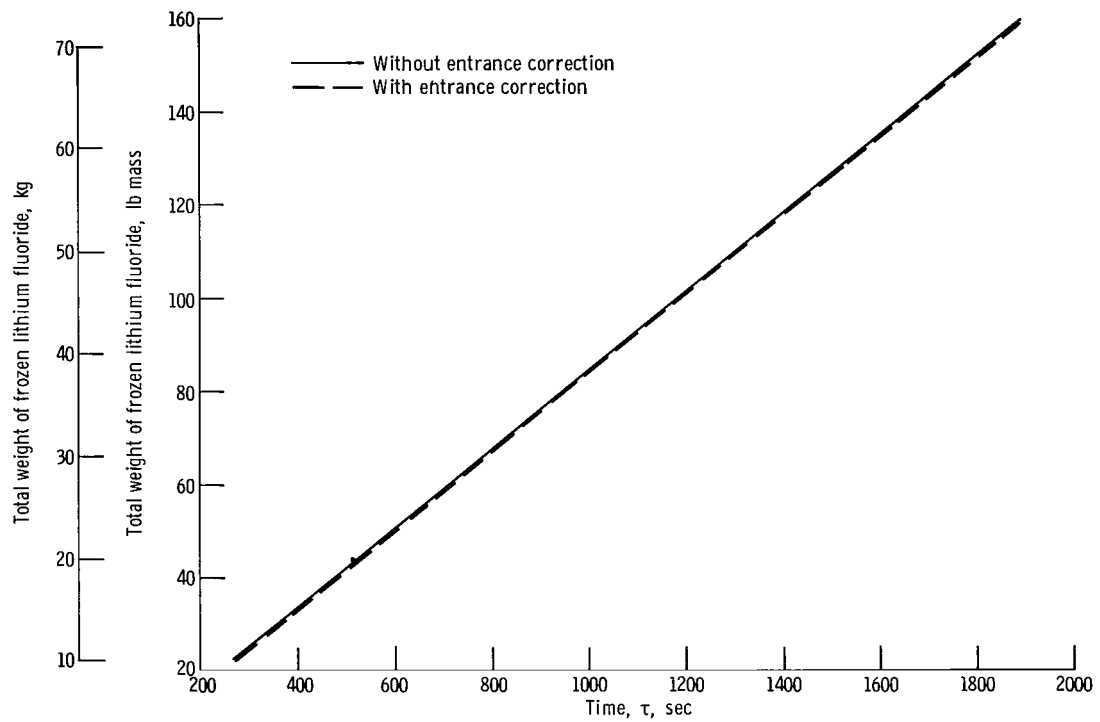


Figure 7. - Weight of frozen lithium fluoride per inch at different stations along tube axis. Tube length, 12.5 feet (3.81 m); tube diameter, 0.087 foot (0.026 m); number of tubes, 30.



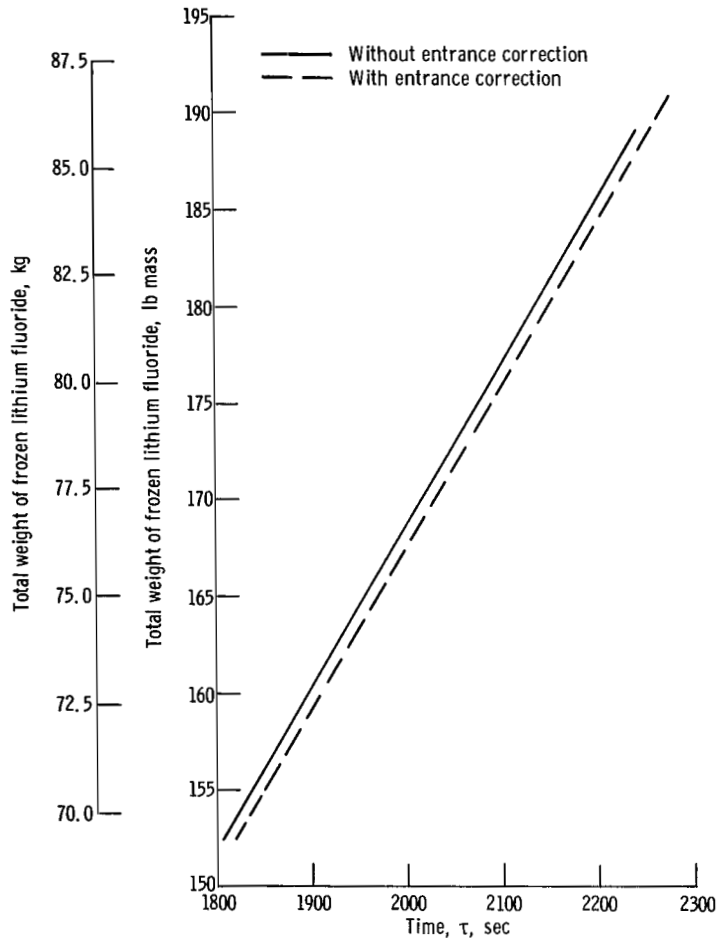
(a) Time, 0 to 160 seconds.

Figure 8. - Variation of total frozen weight of lithium fluoride with time with and without tube entrance correction. Tube length, 12.5 feet (3.81 m); tube diameter, 0.087 foot (0.026 m); number of tubes, 30.



(b) Time, 200 to 2000 seconds.

Figure 8. - Continued.



(c) Time, 1800 to 2300 seconds.

Figure 8. - Concluded.

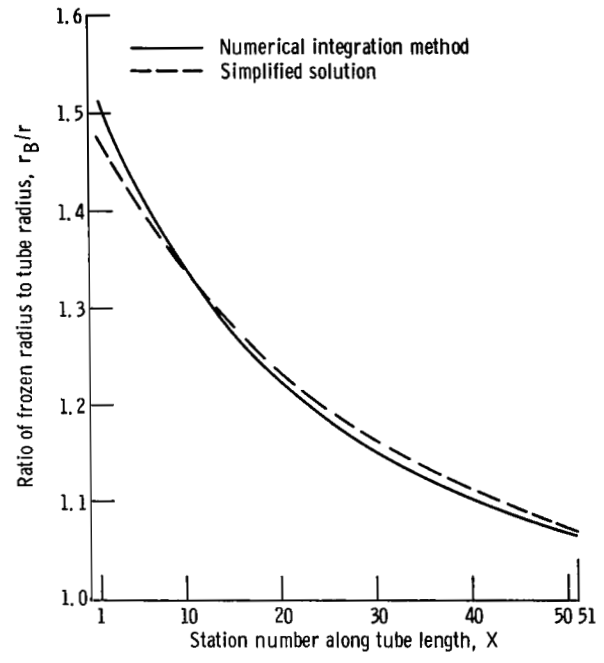


Figure 9. - Comparison of frozen radius ratio for stations along tube axis for numerical integration method and simplified solution. Tube length, 12.5 feet (3.81 m); tube diameter, 0.087 foot (0.026 m); number of tubes, 30; time, 35.3 minutes.

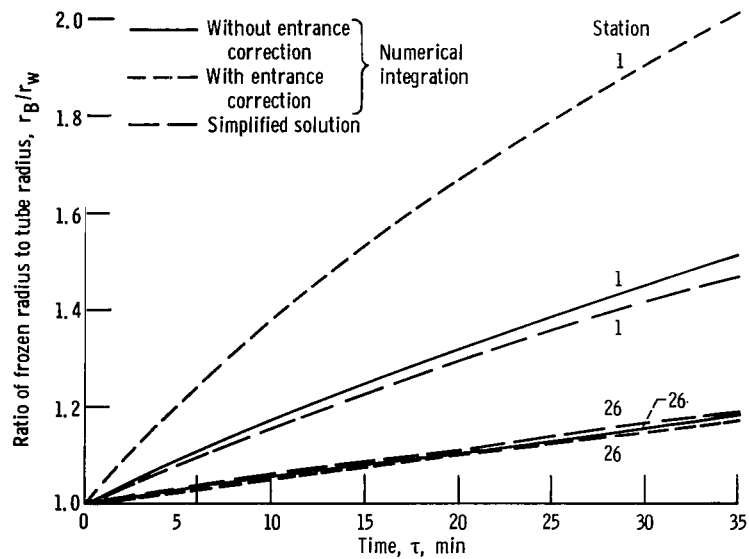


Figure 10. - Comparison of frozen radius ratio with time for numerical integration method with and without entrance correction and simplified solution. Tube length, 12.5 feet (3.81 m); tube diameter, 0.087 foot (0.026 m); number of tubes, 30.

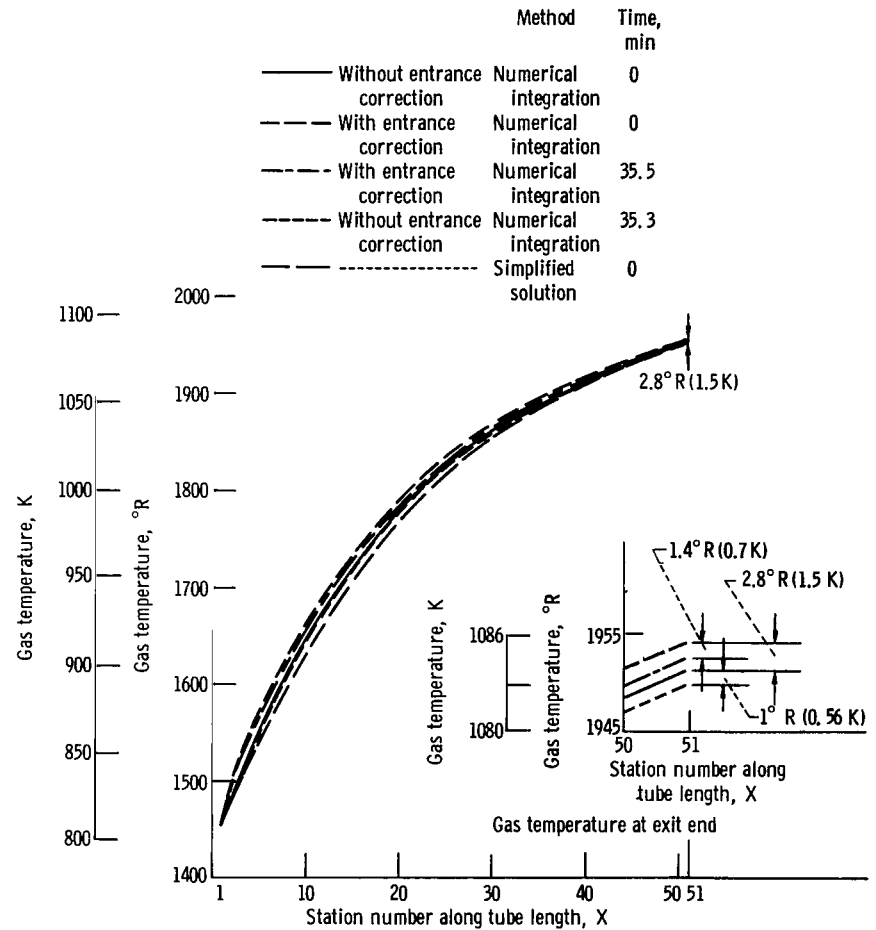


Figure 11. - Comparison of gas temperatures along tube for numerical integration method with and without effect of entrance correction on heat-transfer coefficient and simplified solution. Tube length, 12.5 feet (3.81 m); tube diameter, 0.087 foot (0.026 m); number of tubes, 30.

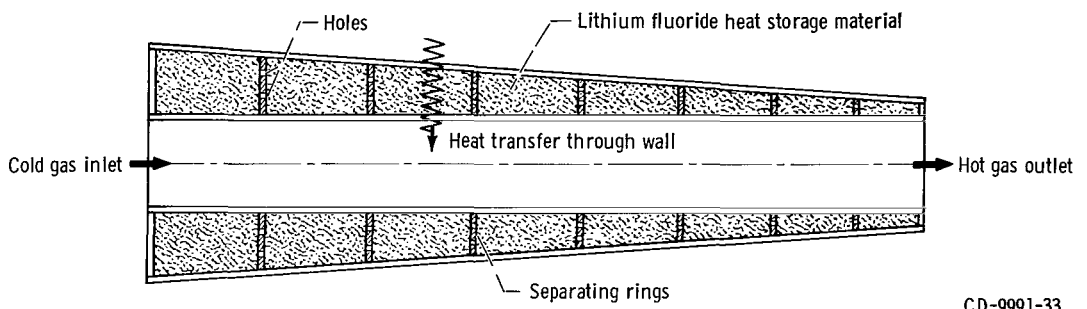


Figure 12. - Tapered outside tube for distribution of thermal-energy-storage material, lithium fluoride.

FIRST CLASS MAIL

060 001 58 01 375 68304 00903
AIR FORCE WEAPONS LABORATORY/AFWL/
KIRTLAND AIR FORCE BASE, NEW MEXICO 87111

SITTING LINDA G. WMAN, ACTING CHIEF TECH. LIAISON

POSTMASTER: If Undeliverable (Section 1
Postal Manual) Do Not Return

"The aeronautical and space activities of the United States shall be conducted so as to contribute . . . to the expansion of human knowledge of phenomena in the atmosphere and space. The Administration shall provide for the widest practicable and appropriate dissemination of information concerning its activities and the results thereof."

— NATIONAL AERONAUTICS AND SPACE ACT OF 1958

NASA SCIENTIFIC AND TECHNICAL PUBLICATIONS

TECHNICAL REPORTS: Scientific and technical information considered important, complete, and a lasting contribution to existing knowledge.

TECHNICAL NOTES: Information less broad in scope but nevertheless of importance as a contribution to existing knowledge.

TECHNICAL MEMORANDUMS: Information receiving limited distribution because of preliminary data, security classification, or other reasons.

CONTRACTOR REPORTS: Scientific and technical information generated under a NASA contract or grant and considered an important contribution to existing knowledge.

TECHNICAL TRANSLATIONS: Information published in a foreign language considered to merit NASA distribution in English.

SPECIAL PUBLICATIONS: Information derived from or of value to NASA activities. Publications include conference proceedings, monographs, data compilations, handbooks, sourcebooks, and special bibliographies.

TECHNOLOGY UTILIZATION PUBLICATIONS: Information on technology used by NASA that may be of particular interest in commercial and other non-aerospace applications. Publications include Tech Briefs, Technology Utilization Reports and Notes, and Technology Surveys.

Details on the availability of these publications may be obtained from:

SCIENTIFIC AND TECHNICAL INFORMATION DIVISION
NATIONAL AERONAUTICS AND SPACE ADMINISTRATION
Washington, D.C. 20546